CHEMICAL ENGINEERING TRANSACTIONS
VOL. 105, 2023
A publication of AIDIC
The Italian Association of Chemical Engineering
Online at www.cetjournal.it
Guest Editors: David Bogle, Flavio Manenti, Piero Salatino

ISBN 979-12-81206-04-5; **ISSN** 2283-9216
DOI: 10.3303/CET23105038

Study of Different H_2/CO_2 Ratios as Feed in Fischer-Tropsch Reactor with Iron-Based Nano-Hydrotalcite Catalysts

Arian Grainca[a,*], Matteo Tommasi[a], Alessandro Di Michele[c], Elisa Zanella[a], Giulia Tonsi[a], Morena Nocchetti[b,d], Carlo Pirola[a,b*]

[a]Università degli Studi di Milano, Dipartimento di Chimica, Milano (Italy)
[b]National Interuniversity Consortium of Materials Science and Technology (INSTM), Florence, Italy
[c]Università di Perugia, Dipartimento di Fisica e Geologia, Perugia (Italy)
[d]Università di Perugia, Dipartimento di Scienze Farmaceutiche, Perugia (Italy)
arian.grainca@unimi.it

CO_2-FTS is among the most viable methods for converting CO_2 into useful chemicals and fuels in order to minimize CO_2 emissions. Due to its chemical inertness, however, effective conversion continues to be a difficulty. The challenges in terms of yield and mechanism have attracted the interest of different research groups in the development of a new carbon dioxide hydrogenation catalysts, capable of reaching satisfactory results. In this work, a selection of nano ternary hydrotalcites (HTlc) were synthesized with and without ultrasound in order to develop active Fe-based catalysts for the Fischer–Tropsch synthesis. HTlc consists mostly of metal hydroxides in which different metal atoms are uniformly distributed at the atomic level. The reaction was carried in a lab scale plant in a fixed bed configuration. All fresh and used catalysts were examined and characterized using XRPD, ICP-OES, SEM, TEM, BET. Ternary HTlc composed of Mg, Cu, and Fe was synthesized using an ultrasound-assisted co-precipitation technique (MCF-US). HTlc was tested for carbon dioxide hydrogenation reaction with a study concerning different H_2/CO_2 ratios in order to evaluate the product distribution as well as the efficiency of the catalyst itself. The CO_2 conversion resulted higher and more stable in feeds with higher H_2 quantities. The selectivity towards higher chain hydrocarbons was higher for lower H_2/CO_2 ratios whereas methane and carbon monoxide selectivities were adequately low.

1. Introduction

Emission of CO_2 due to the use of fossil fuel is widely recognized as the main anthropogenic contribution to the climate change. In recent years, the words green and energy transition have become increasingly popular and this reflect the increasing awareness of the population about this topic. The development of sustainable processes is now also identified as marketing and economic opportunity for the companies. Considerable efforts have been made to reduce carbon dioxide emission into the atmosphere through carbon capture technology (Hasanbeigi et al., 2012). Based on the destination of the captured carbon dioxide, two macro-areas of research are defined: carbon capture and storage (CCS) and carbon capture utilization (CCU). The latter has noticed an increasing attention during the last decade due to the possibility of catalytically transform the captured CO_2 into value added chemical and fuels that can produce further economic profit (Ghosh et al., 2019). Different chemical-conversion-based CCU technology have been proposed to chemically reduce CO_2 to different products. Power-to-gas technology (PTG), where CO_2 is converted to methane (Ghaib et al., 2016), or power to liquid ones (PTL) able to produce commodities chemicals, such as methanol, and fuels (i.e. gasoline, diesel and kerosene) have been studied (Panzone et al., 2020). Since liquid products are easier to handle, store and transport due to their high energy density per volume, PTL strategy is often preferred for medium/long time storage. The production of hydrocarbon fuels from renewable resources has seen a huge increase in popularity in the last decade and the possibility of using CO_2 as a C_1 feedstock commodity is particularly interesting since it allows to couple the demand for green fuel from one side and the utilization of the captured CO_2 (Ryu et al., 2022). Fischer Tropsch synthesis (FTS) represents one of the main processes in the hydrocarbons production

Paper Received: 21 January 2023; Revised: 13 July 2023; Accepted: 6 June 2023
Please cite this article as: Grainca A., Tommasi M., Di Michele A., Zanella E., Tonsi G., Nocchetti M., Pirola C., 2023, Study of Different H_2/CO_2 Ratios as Feed in Fischer-Tropsch Reactor with Iron-Based Nano-Hydrotalcite Catalysts, Chemical Engineering Transactions, 105, 223-228 DOI:10.3303/CET23105038

field. Since its discovery, in 1925, it has been the subject of research given the possibility of obtaining a wide range of products, consisting mainly of alfa-olefins and linear paraffins, without sulphur, nitrogen and aromatics compounds. The versality of the raw material used for this process is one of the reasons why it's still extremely interesting to these days. Originally performed with the use of syngas, produced through gasification of the coal (CTL) (Mohajerani et al., 2018), different raw material such as natural gas and biomass have been studied (Fei et al., 2014; Luque et al., 2012). Lately scientific research focused on the CO_2 based FTS, which can utilize captured carbon dioxide in order to obtain high quality FT fuels, such as diesel that could be used also in countries with stringent specifications (Martín & Cirujano, 2022). Compared to classical Fischer Tropsch, when using H_2-CO_2 mixture as input, the synthesis goes through two distinct reactions: the Reverse Water Gas Shift Reaction (RWGS) (Eq. 1) and the subsequent Fisher Tropsch synthesis (Eq. 2), which are endothermic and exothermic respectively.

$$CO_2 + H_2 \rightarrow CO + H_2O \quad \Delta H_{573K} = 38 \left({}^{kJ}/_{mol}\right) \tag{1}$$

$$CO + 2H_2 \rightarrow -CH_2 - + H_2O \quad \Delta H_{573K} = -166 \left({}^{kJ}/_{mol}\right) \tag{2}$$

FTS from CO_2 can therefore be conducted in two different ways: the so-called indirect route, where the RWGS and the FTS reaction take place in two different reactors, and via direct route, where both reactions are run in the same reactor. The former relies primarily on highly selective cobalt-based catalysts to produce heavy hydrocarbons. However, when working with a direct CO_2-FTS, Fe-based catalyst are preferred over cobalt ones due to their higher activity towards the RWGS reaction. When used in high-temperature reactors, Fe-based catalysts also allow high selectivity towards olefins, yielding a product composed of high calorie SNG and hydrocarbons (Gao et al., 2021). Additionally, they permit obtaining shorter paraffins and olefins which can be separated into the different fraction (gasoline, diesel and kerosene) without the need of further treatment (i.e., hydrocracking) as needed to upgrade longer fractions. The addition of potassium to iron-based catalysts promotes the reduction of CO_2 in hydrocarbon chains. K acts as an electronic promoter for Fe-based catalysts and this make possible to achieve an increase in CO_2 conversion and a reduction in the formation of short-chain hydrocarbon compounds (Li et al., 2001).

As a new catalyst for the CO_2 hydrogenation process, here is proposed double and triple-layered hydroxides, also known as hydrotalcite-like compounds (HTlc). Specifically, this iron-based hydrotalcite was studied in a classical CO FTS with great results (Grainca A., 2022), therefore the decision to test also CO2 hydrogenation. HTlc is mostly composed of metal hydroxides in which particular metal atoms are uniformly scattered at the atomic level. $[M(II)_{1-x}M(III)_x(OH)_2{}^{x+}[A_{n-\,x/n}]^{x-}mH_2O\,]$ is the formula that represents HTlc, where M(II) is a divalent cation like Co, Mg, Zn, Ni, or Cu; M(III) is a trivalent cation like Al, Cr, Fe, or Ga; An is an anion with charge n; and m is the molar quantity of co-intercalated water. FTS are assumed to adhere to the Anderson-Schulz-Flory (ASF) distribution, which is based on the likelihood of chain formation (α) (Chen & Yang, 2019; Stenger & Askonas, 1986). To determine the influence of the H_2/CO_2 ratio and the GHSV on the product distribution, MgCuFe-K catalyst has been evaluated under several conditions.

2. Experimental

2.1 Catalyst synthesis

The MgCuFe-US sample was prepared using an ultrasound-assisted co-precipitation technique. 50 mL of NaOH 1M and $NaHCO_3$ 2M solution was added dropwise to 56 mL of Mg, Fe, and Cu nitrate salts 1 M solution (Mg/Fe/Cu molar ratio = 13.2/6.3/1). Throughout the addition procedure, the solutions were ultrasonically agitated at 20 kHz for 3.5 minutes, and the temperature of the sample was maintained at 278 K. Immediately, a yellow-brown solid precipitated. The precipitate was diluted with 100 mL of distilled water once the addition was completed. The solid was recovered using centrifugation, washed many times with deionized water, and then dried in an oven at 333 K. The final composition of MgCuFe-US, as measured by ICO-OES, is $[Mg_{0.67}Cu_{0.045}Fe_{0.29}(OH)_2].\ (CO_3)_{0.15}\ 0.5\ H_2O$.

2.2 Characterization Techniques

XRD patterns of powdered materials were acquired using an X'PERT PRO diffractometer (PanAlytical, Roiston, UK) operating at 40 kV and 40 mA with an X'Celerator detector. The 3-70(°) 2θ measurement range was obtained using a 0.030° 2θ step size and 30 s step scan. A 700-ES series inductively coupled plasma optical emission (ICP-OES) spectrometer was used to evaluate the metal content of samples (Varian, Santa Clara, CA, USA). In a total volume of 100 mL, 5 mg of each sample was dissolved in concentrated HNO_3 and purified water was added. Field emission scanning electron microscopy LEO 1525 was used to assess the morphology of the materials (ZEISS). The sample was placed using conductive carbon adhesive tape on an aluminum support.

The samples were coated with a thin coating of chromium prior to examination (8 nm). At 15 kV, measurements were performed using an In-lens detector. Using a Bruker Quantax EDX, the elemental composition and chemical mapping of the sample were determined. With the use of a Philips 208 Transmission Electron Microscope, TEM pictures were acquired. The samples were made by applying one drop of an ethanol dispersion of the catalyst powder to a Formvar-coated copper grid and drying it in air.

3. Experimental setup

In a continuous mixer, three Brooks mass flow controllers measured the flow of H_2 (30 Nml min^{-1}, 99.9% purity), CO_2 (10 Nml min^{-1}, 99.9% purity), and N_2 (internal standard, 5 Nml min^{-1}, 99.99% purity). The mixture was introduced from the top of a packed bed reactor with an internal diameter of 6 mm and 1 g of catalyst. The catalyst bed was held in place by two pieces of quartz wool and a blank test ensured that its inside surface was inert. The temperature of the reactor was measured by a K-type thermocouple, which was heated by an oven. A second thermocouple of type K monitored the interior temperature of the reactor. The activation of the catalyst was conducted at 623 K and 0.4 MPa for four hours with the same reagent flow (45 Nml min^{-1}) and CO_2/H_2. After condensing liquid products (water and C_{7+}) in a 0.13 L cold trap with an external cooling jacket at 278 K, they were examined by gas chromatography. Using a pneumatic back pressure regulator, the pressure was maintained at 2.0 MPa. Using an Agilent 3000A micro gas chromatograph, N_2 and CO_2 peak areas (AN_2, and ACO_2), their relative response factor (k), and the inlet (set) flowrate of N_2 and CO_2 (Fin N2, and Fin, CO_2) were measured to calculate CO_2 conversion (X CO_2) (Eq. 3).

$$X_{CO2} = \frac{F_{in,CO2} - F_{in,N_2}}{F_{in,CO2}} \times k \frac{A_{CO}2}{A_{N_2}} \quad (3)$$

The analyzer, which was equipped with molsieve and QPLOT columns, collected effluent samples every two hours. Each FT run had its mass and molar compositions balanced, with a 5% molar basis error being the absolute limit. The catalyst was analyzed for its characteristics both before and after the activation process was carried out in the reactor. "Fresh catalysts" refers to samples that were produced prior to activation. "Activated catalysts" refers to samples that were activated in the FTS reactor via the reduction activation technique and then removed from the reactor.

4. Results and Discussion

4.1 Materials Characterization

The diagram in Figure1 illustrates the XRD patterns of MgCuFe-LDH. X-ray diffraction is the most widely utilized method for characterizing the multilayer structure of HTs. In this instance, nanosized structures exhibit XRD patterns that are wider and also represent the creation of smaller crystallites.

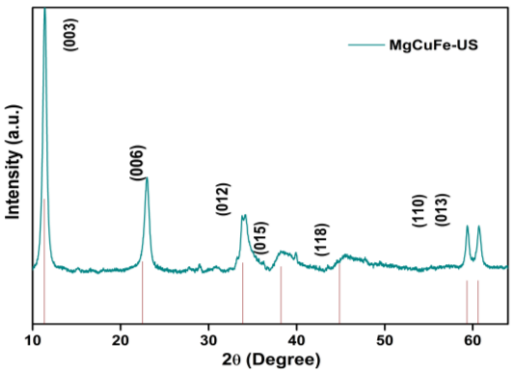

Figure 1: X-ray diffractogram of as synthetized MgCuFe US

Peaks detected at 11.38°, 23.02°, 34.62°, 59.34°, and 60.62° were attributed to (003), (006), (012), (110), and (013) planes, which are typical peaks of hydrotalcite-like compounds; also, the interlayer space of HTlc harbors carbonate ions, as shown by the location of the initial reflection at 2 = 11.7°.

Specifically, the (003), (006) and (012) diffraction peaks can indicate whether or not the hydrotalcite compounds have layered structures. It has been shown that the lattice parameter c (23.41 Å) depends on the thickness of the octahedral sheet, the thickness of the anion sheet, and the intensity of the electrostatic attraction between the sheets. Unlike conventional MgAl-HT, which has a lattice value of c equal to 22.80, MgFe-HT has a lattice parameter of c equal to 23.41 Å, which explains the enlargement of the hydrotalcitic structure. Notably, in the MgCuFe-US pattern, a peak at 2 = 32.3°, denoted with an asterisk, is likely attributable to a remnant of a Na-

containing molecule, as found by EDS analysis. Using Debye-Scherrer equation the average size of the catalyst was estimated (Eq. 4):

$$y = \frac{0.9\lambda}{\beta cos\theta} \quad (4)$$

where λ is the wavelength source (for Cu Kα = 40 kV, 30 mA), θ is the Bergg diffraction angle and β is the breadth of the XRD peak at half maximum height. The crystallite size of MgFe-LDH was thus determined to be 37 nm.

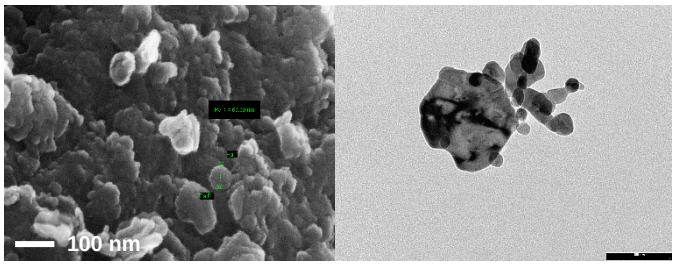

Figure 2: SEM (a) and TEM (b) images of MgCuFe-US

The existence of hydrotalcitic structure is confirmed by the appearance of flat and hexagonal platelets in SEM and TEM images (Figure 4a) of the MgCuFe-US sample. As previously shown in the XRD spectra, the size distribution of crystals is not homogenous; the samples are characterized by nanosized aggregates. Compared to the Debye-Scherrer equations, the XRD investigation reveals platelets in the 40-70 nm nm range.
Analysis regarding the surface area reveal a value of 87.2 m^2/g for the fresh sample, which is in accordance with values for the same class of HTLc. Interesting results arise when the same analysis is performed after the activation, that shows a decrease in surface area and cumulative pore volume against a major presence of larger pore. This might be explained due to the breaking of the structure at high temperature, typically 673 K, which is close to the activating one at 623 K, leading to the collapse of smaller pores, thus increasing the average pore diameter but diminishing the overall sum of pore volumes.

Table 2 BET specific surface area

Sample	Specific surface area (m^2/g)	Cumulative pore volume (cm^3/g)	Average pore diameter (Å)
MgCuFe fresh	85	0.35	160
MgCuFe activated	31	0.23	258

4.2 ASF distribution

Products obtained from FTS are assumed to follow the Anderson-Schulz-Flory (ASF) distribution which is characterized by a chain growth probability (α). It can be mathematically translated as the ratio between the chain propagation rate and the sum of this rate with the chain termination (Eq. 5) (Chen & Yang, 2019; Stenger & Askonas, 1986). It is therefore also possible to calculate the probability that the chain desorbs from the catalyst as it's shown in (Eq. 6). Consequently, it is possible to calculate the probability of formation of a compound containing n carbon atoms, and its relative weight fraction (w_n) over the entire product spectrum (Eq. 7).

$$\alpha = \frac{r_p}{r_p + r_t} \quad (5)$$

$$1 - \alpha = \frac{r_t}{r_p + r_t} \quad (6)$$

$$\frac{w_n}{n} = (1-\alpha)^2 \cdot \alpha^{n-1} \quad (7)$$

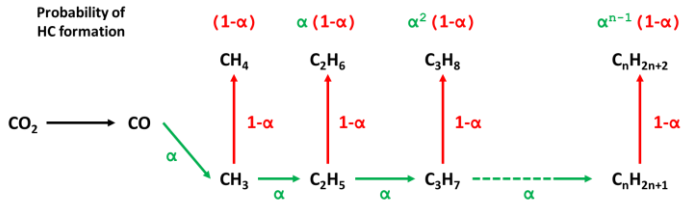

Figure 3: Probability of hydrocarbon formation

In Figure 3 a visual representation of the probability of formation of different products is displayed (Panahi et al., 2012). From (Eq. 7) it's possible to obtain a linear relationship (Eq. 8) between the carbon number of a product and its relative weight fraction.

$$\ln\left(\frac{w_n}{n}\right) = \ln(1-\alpha)^2 + (n-1)\cdot\ln\alpha \quad (8)$$

The chain growth probability (α) can be regressed from the obtained semilogarithmic graphs and defines the spectra of the products obtained. The higher the α, the longer the hydrocarbons chains. α depends on several factors, such as the type of the catalyst and the process conditions adopted. In this work the effect of H_2/CO_2 ratio and GHSV over the chain growth probability have been studied. The ASF equation, through the chain growth probability, gives a primary approximation of the products distribution but there are some drawbacks. The main problems relate to the methane selectivity: usually CH_4 selectivity predicted by ASF model is lower than the one measured experimentally. Some authors claimed that the high CH_4 selectivity is induced by a higher rate constant for methane compared to the rate constant of heavier products (Ma et al., 2014). The greater constant rates are attributable to a larger pre-exponential factor for methane desorption relative to other products, although activation energies seem similar (Visconti et al., 2011). Furthermore, the expected selectivity to C_2 portion by the ASF is close to 30% wt, although experimental values barely approach 18%wt. This difference might be caused by a number of factors, the most credible being the incorporation or hydrolysis of ethylene (Yang et al., 2014).

4.3 Experimental results

For reasons previously mentioned, methane and C_2 fractions have been excluded from the ASF calculation. Points represent experimental data, and solid lines fits to the α distribution. The chain growth probability has been obtained by the angular coefficient of the straight line.

The results obtained during a typical run under reference conditions (H_2/CO_2 molar inlet ratio = 3, 20 bar, 573 K, GHSV = NmL g_{cat}^{-1} h^{-1}) are reported in Figure 6. Figure 6b and 6c show the chain probability obtained varying respectively the feed ratio H_2/CO_2=4 and the space velocity which has been doubled from 1600 to 3200 Nml g_{cat}^{-1} h^{-1}.

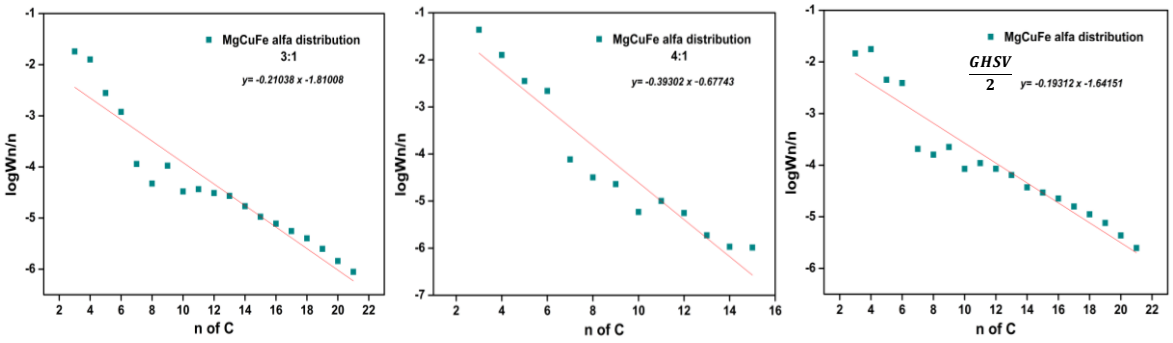

Figure 4: hydrocarbon chain distribution, a) 3 to 1 H_2/CO_2 ratio, b) 4 to 1 ratio, c) doubled residence time.

Table 3: Reaction conditions and overall conversion

Sample	Feed ratio H_2/CO_2	GHSV (Nml g_{cat}^{-1} h^{-1})	CO_2 conv %	α
MgCuFe 3/1	3	3200	34.2	0.61
MgCuFe 4/1	4	3200	33.3	0.40
MgCuFe GHSV/2	3	1600	44.8	0.64

As can be evaluated from the trend lines: increasing the molar inlet of hydrogen the probability of chain growth decreases, yielding a higher production of shorter hydrocarbon chains (C_{3-7}).

On the contrary when doubling the GHSV value, the chain growth probability increases as the contact time between the feed mixture and the active sites is major.

The relations between GHSV, inlet feed ratios and hydrocarbon distribution display similar trend to the classical Fischer-Tropsch reaction (Mohajeri et al., 2014; Yang et al., 2014). Satisfactory results were obtained regarding the conversions of CO_2, with the highest being the run performed with doubled residence time for kinetic reasons. As for the comparison between the increasing feed ratios, the final conversions are very similar with changes in the selectivities of CO, considerably higher for the H_2/CO_2=4 at 25.1% against the 18.5% of the lower hydrogen ratio feed. As expected, the selectivity towards C_{7+} increases.

5. Conclusions

Novel Fe-based compounds resembling hydrotalcite were produced and used as catalysts for the hydrogenation of CO_2 using a Fischer–Tropsch synthesis route. The catalyst was synthesized using an ultrasound-assisted technique, and several reaction temperatures were examined before settling on 573 K as the optimal working temperature. This study's objective was to evaluate the application of this new type of catalysts in the carbon dioxide hydrogenation reaction and to compare different feed ratios, from 3/1 to 4/1 H_2/CO_2 and different space velocities, from 3200 to 1600 Nml g_{cat}^{-1} h^{-1}, which resulted in a similar capacity for CO_2 conversion but observable differences in the distribution of hydrocarbons. As anticipated, the catalytic activity of the samples is reliant on the GHSV. The basic scenario of H_2/CO_2=3, GHSV= 3200 Nml g_{cat}^{-1} h^{-1} exhibited almost equal CO_2 conversion to the equivalent 4 to 1 ratio, with variations in selectivities resulting in a greater proportion of light hydrocarbon phase for the latter. In contrast, when the basic case was examined with the same inflow ratio at half the initial GHSV, both conversion and heavy hydrocarbon propagation increased. As a consequence of the encouraging findings, more research on HTLc as a catalytic material will be conducted. The ensuing study will entail examining the impacts of various characteristics, such as crystallite form and size, and altering the stoichiometric amounts of the catalyst itself.

References

Chen, J., & Yang, C. (2019). Thermodynamic Equilibrium Analysis of Product Distribution in the Fischer-Tropsch Process under Different Operating Conditions. ACS Omega, 4(26), 22237–22244.

Fei, Q., Guarnieri, M. T., Tao, L., Laurens, L. M. L., Dowe, N., & Pienkos, P. T. (2014). Bioconversion of natural gas to liquid fuel: Opportunities and challenges. Biotechnology Advances, 32(3), 596–614.

Gao, R. et al. (2021). Green liquid fuel and synthetic natural gas production via CO2 hydrogenation combined with reverse water-gas-shift and Co-based Fischer-Tropsch synthesis. Journal of CO2 Utilization, 51(April).

Ghaib, K., Nitz, K., & Ben-Fares, F. Z. (2016). Chemical methanation of CO2: A review. ChemBioEng Reviews, 3(6), 266–275.

Ghosh, S., Uday, V., Giri, A., & Srinivas, S. (2019). Biogas to methanol: A comparison of conversion processes involving direct carbon dioxide hydrogenation and via reverse water gas shift reaction. Journal of Cleaner Production, 217, 615–626.

Grainca, A. et al (2022). Iron based nano-hydrotalcites promoted with Cu as catalysts for Fischer-Tropsch synthesis in biomass to liquid process. CEt CHEMICAL ENGINEERING TRANSACTIONS, vol 96.

Hasanbeigi, A., Price, L., & Lin, E. (2012). Emerging energy-efficiency and CO 2 emission-reduction technologies for cement and concrete production: A technical review. Renewable and Sustainable Energy Reviews, 16(8), 6220–6238.

Li, S., Li, A., Krishnamoorthy, S., & Iglesia, E. (2001). Effects of Zn, Cu, and K promoters on the structure and on the reduction, carburization, and catalytic behavior of iron-based Fischer-Tropsch synthesis catalysts. Catalysis Letters, 77(4), 197–205.

Luque, R., et al (2012). Design and development of catalysts for Biomass-To-Liquid-Fischer-Tropsch (BTL-FT) processes for biofuels production. Energy and Environmental Science, 5(1), 5186–5202.

Ma, W., Jacobs, G., Sparks, D. E., Spicer, R. L., Davis, B. H., Klettlinger, J., Yen, C. H. (2014). Fischer-Tropsch synthesis: Kinetics and water effect study over 25%Co/Al2O3 catalysts. Catalysis Today, 228, 158–166.

Martín, N., & Cirujano, F. G. (2022). Multifunctional heterogeneous catalysts for the tandem CO2hydrogenation-Fischer Tropsch synthesis of gasoline. Journal of CO2 Utilization, 65(August), 102176.

Mohajerani, S., Kumar, A., & Oni, A. O. (2018). A techno-economic assessment of gas-to-liquid and coal-to-liquid plants through the development of scale factors. Energy, 150, 681–693.

Mohajeri, A., Zamani, Y., & Shirazi, L. (2014). Investigation of Products Distribution In Fischer-Tropsch Synthesis By Nano-sized Iron-based Catalyst. 1–7.

Panahi, M., Rafiee, A., Skogestad, S., & Hillestad, M. (2012). A natural gas to liquids process model for optimal operation. Industrial and Engineering Chemistry Research, 51(1), 425–433.

Panzone, C. et al (2020). Power-to-Liquid catalytic CO2 valorization into fuels and chemicals: Focus on the Fischer-Tropsch route. Journal of CO2 Utilization, 38(September 2019), 314–347.

Ryu, K. H., Kim, B., & Heo, S. (2022). Sustainability analysis framework based on global market dynamics: A carbon capture and utilization industry case. Renewable and Sustainable Energy Reviews, 166(May).

Stenger, H. G., & Askonas, C. F. (1986). Thermodynamic Product Distributions for the Fischer-Tropsch Synthesis. Industrial and Engineering Chemistry Fundamentals, 25(3), 410–413.

Visconti, C. G et al (2011). Detailed kinetics of the fischer-tropsch synthesis on cobalt catalysts based on H-assisted CO activation. Topics in Catalysis, 54(13–15), 786–800.

Yang, J., Ma, W., Chen, D., Holmen, A., & Davis, B. H. (2014). Fischer-Tropsch synthesis: A review of the effect of CO conversion on methane selectivity. Applied Catalysis A: General, 470, 250–260.